BIOCHEMISTRY
including biophysical chemistry & molecular biology
Article

*Biochemistry* **2009,** *48,* 5199–5209 5199
DOI: 10.1021/bi802335s

# Activation of Anthranilate Phosphoribosyltransferase from *Sulfolobus solfataricus* by Removal of Magnesium Inhibition and Acceleration of Product Release[†,‡]

Sandra Schlee,[§] Miriam Deuss,[§,∥] Marc Bruning,[⊥] Andreas Ivens,[∥] Thomas Schwab,[§] Nadja Hellmann,[#] Olga Mayans,[△] and Reinhard Sterner*[,§,∥]

[§]*Institute of Biophysics and Physical Biochemistry, University of Regensburg, Universitätsstrasse 31, D-93053 Regensburg, Germany,* [∥]*Institute of Biochemistry, University of Cologne, Otto-Fischer-Strasse 12-14, D-50674 Cologne, Germany,* [⊥]*Division of Structural Biology, Biozentrum, University of Basel, Klingelbergstrasse 70, CH-4056 Basel, Switzerland,* [#]*Institute of Molecular Biophysics, University of Mainz, Jakob-Welder-Weg 26, D-55128 Mainz, Germany, and* [△]*School of Biological Sciences, University of Liverpool, Crown Street, Liverpool L69 7ZB, U.K.*

*Received December 22, 2008; Revised Manuscript Received April 18, 2009*

ABSTRACT: Anthranilate phosphoribosyltransferase from the hyperthermophilic archaeon *Sulfolobus solfataricus* (ssAnPRT) is encoded by the ss*trp*D gene and catalyzes the reaction of anthranilate (AA) with a complex of $Mg^{2+}$ and 5′-phosphoribosyl-α1-pyrophosphate (Mg·PRPP) to N-(5′-phosphoribosyl)-anthranilate (PRA) and pyrophosphate ($PP_i$) within tryptophan biosynthesis. The ssAnPRT enzyme is highly thermostable (half-life at 85 °C = 35 min) but only marginally active at ambient temperatures (turnover number at 37 °C = 0.33 $s^{-1}$). To understand the reason for the poor catalytic proficiency of ssAnPRT, we have isolated from an ss*trp*D library the activated ssAnPRT-D83G + F149S double mutant by metabolic complementation of an auxotrophic *Escherichia coli* strain. Whereas the activity of purified wild-type ssAnPRT is strongly reduced in the presence of high concentrations of $Mg^{2+}$ ions, this inhibition is no longer observed in the double mutant and the ssAnPRT-D83G single mutant. The comparison of the crystal structures of activated and wild-type ssAnPRT shows that the D83G mutation alters the binding mode of the substrate Mg·PRPP. Analysis of PRPP and $Mg^{2+}$-dependent enzymatic activity indicates that this leads to a decreased affinity for a second $Mg^{2+}$ ion and thus reduces the concentration of enzymes with the inhibitory $Mg_2$·PRPP complex bound to the active site. Moreover, the turnover number of the double mutant ssAnPRT-D83G + F149S is elevated 40-fold compared to the wild-type enzyme, which can be attributed to an accelerated release of the product PRA. This effect appears to be mainly caused by an increased conformational flexibility induced by the F149S mutation, a hypothesis which is supported by the reduced thermal stability of the ssAnPRT-F149S single mutant.

Naturally occurring enzymes must be significantly stable in order to maintain their native conformations but also sufficiently flexible to fulfill their manifold catalytic activities. Unraveling the relationship between structure, function, and stability of enzymes is relevant, because it will eventually allow us to design enzymes with a desired combination of stability and activity (*1*). Important insights into this problem were obtained by comparative investigations of extremely stable enzymes from hyperthermophiles and their labile homologues from mesophiles (*2*). Enzymes from hyperthermophiles, which optimally grow close to the boiling point of water, often are barely active at room temperature but are as active as their mesophilic counterparts at the corresponding physiological temperatures. It has been postulated that the low activity of most thermostable enzymes at mesophilic temperatures is due to a high structural rigidity, which is relieved at the elevated temperatures at which hyperthermophilic enzymes work *in vivo* [concept of "corresponding states" (*3*)]. The rarely found combination of high thermostability and high catalytic activity at low temperature in native enzymes is probably due to a lack of evolutionary constraints (*4*). Enzymes in mesophilic organisms are under no selective pressure to be stable at elevated temperature. Similarly, the activities of hyperthermophilic enzymes at low temperatures normally need not to be high. Otherwise, hyperthermophilic enzymes would be much more efficient catalysts than their mesophilic homologues at the corresponding optimum growth temperatures, due to the acceleration of chemical reactions with increasing temperature. An example are two $(\beta\alpha)_8$-barrel enzymes from the hyperthermophile *Thermotoga maritima*, namely, phosphoribosylanthranilate isomerase and *N*′-[(5′-phosphoribosyl)formimino]-5-aminoimidazole-4-carboxamide ribonucleotide isomerase, which need to be extremely active at their physiological temperatures in order to outrun the spontaneous degradation of their thermolabile substrates (*5*, *6*).

One approach to unravel the mutual interdependence of catalytic activity and conformational stability is the generation

[†]This work was supported by grants of the Deutsche Forschungsgemeinschaft (SPP1170: STE 891/5-1, 5-2, 5-3) and a fellowship of the Bayerische Eliteförderung to S.S.

[‡]Structure factor amplitudes and model coordinates of ssAnPRT-D83G + F149S have been deposited at the Protein Data Bank with accession code 3GBR.

*Corresponding author. Phone: +49 941-943 3015. Fax: +49 941-943 2813. E-mail: Reinhard.Sterner@biologie.uni-regensburg.de.

 Published on Web 04/22/2009 

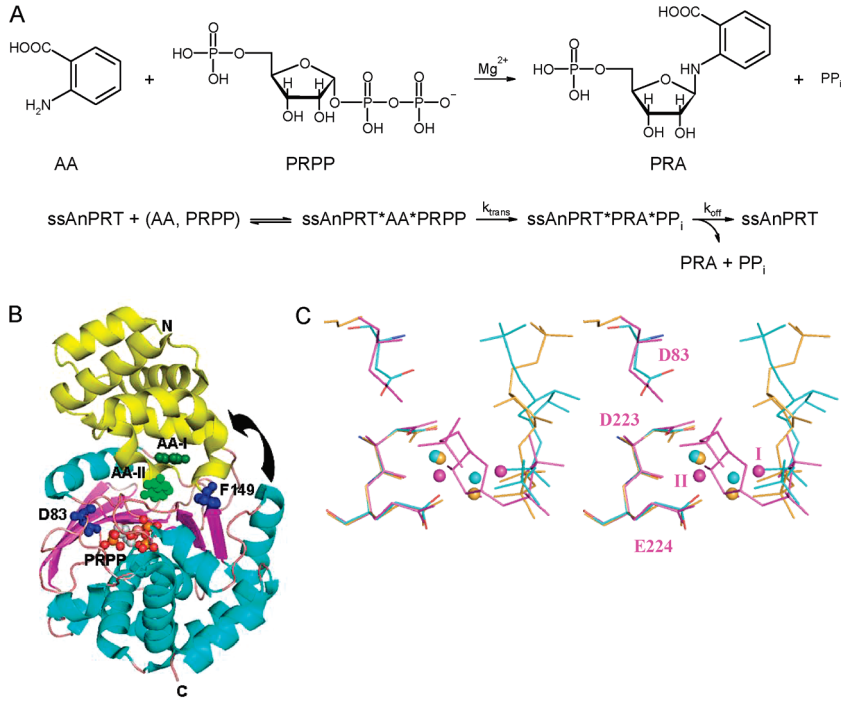


FIGURE 1: Catalyzed reaction and crystal structures of anthranilate phosphoribosyltransferases. (A) Upper panel: Reaction catalyzed by ssAnPRT. Abbreviations: AA, anthranilate; PRPP, 5′-phosphoribosyl-α1-pyrophosphate; PRA, *N*-(5′-phosphoribosyl)anthranilate; $PP_i$, pyrophosphate. Lower panel: Minimal catalytic mechanism of the reaction. (B) Ribbon diagram of the X-ray structure of wild-type ssAnPRT with bound substrates. Coordinates were obtained from PDB entry 1ZYK. For clarity, only one protomer of the homodimer is shown. The N- and C-termini of the polypeptide chain are labeled. Protein domains are color-coded where the small N-terminal α-domain is yellow and the large C-terminal α/*β*-domain is purple and cyan. The two bound anthranilate molecules (AA-I and AA-II) are in green; bound PRPP is in gray (ribose moiety) and orange/red (phosphate moieties). Residues aspartate 83 and phenylalanine 149, which are substituted in the activated variant by glycine and serine, are displayed in blue. A putative domain motion upon substrate binding and product release is indicated by an arrow. (C) Stereoplot of PRPP and metal coordination by ssAnPRT-wt (magenta), ssAnPRT-D83G + F149S (golden), and mtAnPRT (cyan). The structures have been superimposed on the main chain atoms of the conserved acidic motif (D223-E224 in ssAnPRT). Residue numbers and location of the two bound metals (I, II) are indicated for ssAnPRT-wt. Stereo is in focused mode.

of enzymes with altered properties, either by rational protein design or by directed evolution. Such experiments have shown that enzyme mutants with improved catalytic activities compared to the wild-type enzyme often display reduced conformational stabilities (*7*−*12*) but that an increase in stability does not necessarily lead to a decrease in enzymatic activity (*13*−*18*). In most cases, however, the structural basis of simultaneous changes in activity, stability, and flexibility has remained unclear.

The members of the family of phosphoribosyltransferases (PRTases) are involved in the metabolism of nucleotides and amino acids. PRTases catalyze the $Mg^{2+}$-dependent displacement of pyrophosphate ($PP_i$)[1] from 5′-phosphoribosyl-α1-pyrophosphate (PRPP) by a nitrogen-containing nucleophile, producing an α-substituted ribose 5-phosphate (*19*). On the basis of their tertiary structures, PRTases have been divided into different classes. Known members of class I are the orotate and uracil PRTases (*20*−*22*), as well as the purine PRTases, which transfer ribose 5-phosphate onto adenine, guanine, hypoxanthine, or xanthine (*23*). Representatives of class II are the quinolinate and nicotinic acid PRTases (*24*, *25*).

Anthranilate PRTase (AnPRT) catalyzes the third step within the biosynthesis of tryptophan, which is the reaction of anthranilate (AA) with Mg·PRPP, yielding phosphoribosyl anthranilate (PRA) and $PP_i$ (Figure 1A). The X-ray structures of the homodimeric AnPRT enzymes from *Sulfolobus solfataricus* (ssAnPRT) (*26*, *27*), *Pectobacterium carotovorum* (*28*), *Mycobacterium tuberculosis* (*29*), *Thermus thermophilus* (PDB entry 1V8G), and *Nostoc* sp. (PDB entry 1VQU) have been solved at high resolution. Their analysis revealed a novel PRTase fold, which is different from the folds of both class I and class II PRTases but similar to that of nucleoside phosphorylases. The AnPRT protomer consists of two domains, a small N-terminal α-helical domain and a large C-terminal α/*β*-domain, which are connected by a hinge region (Figure 1B). The two substrates AA and Mg·PRPP bind into two different domains within each protomer and are brought together during catalysis by rotational domain motions (*26*). Loosening of the dimer by exchanging two hydrophobic residues at the interface with negatively charged ones yielded a monomeric ssAnPRT mutant with unaltered enzymatic activity but reduced thermal stability (*30*).

The wild-type ssAnPRT enzyme is extremely thermostable with a half-life at 85 °C of 35 min (*31*) and catalytically proficient at 60 °C with a turnover number of 4.2 $s^{-1}$ (*26*) but only marginally active at 37 °C with a turnover number of 0.33 $s^{-1}$. The aim of our study was to generate ssAnPRT mutants with an increased activity at ambient temperature. We then wanted to elucidate the mechanism of activation and to analyze the consequences for thermal stability. We first generated an ss*trp*D gene library from which we isolated the activated ssAnPRT-D83G + F149S double mutant by *in vivo* complementation of an auxotrophic *Escherichia coli* strain at 37 °C. Subsequent steady-state and transient enzyme kinetic measurements, X-ray structure analysis, and thermal unfolding studies suggest that the

[1]Abbreviations: AA, anthranilate; AnPRT, anthranilate phosphoribosyltransferase; $PP_i$, pyrophosphate; PRPP, 5′-phosphoribosyl-α1-pyrophosphate; mtAnPRT, AnPRT from *Mycobacterium tuberculosis*; ssAnPRT, AnPRT from *Sulfolobus solfataricus*; ss*trp*D, gene encoding ssAnPRT; wt, wild type.

activating effect of the mutations is based on different mechanisms. The D83G exchange relieves the strong inhibition of wild-type ssAnPRT by the $Mg_2$·PRPP complex that forms on the enzyme at high concentrations of $Mg^{2+}$, whereas the destabilizing F149S exchange appears to facilitate product release by increasing the conformational flexibility of the enzyme.

## EXPERIMENTAL PROCEDURES

*Generation of a Plasmid Library of sstrpD Genes by DNA Shuffling (32)*. The ss*trp*D gene was amplified by PCR with Taq DNA polymerase, using pQE40-ss*trpD* plasmid as the template (*31*), and the oligonucleotides CyRI and CyPst (*33*) as 5′- and 3′-primers, respectively. The following amplification conditions were applied: step 1, 95 °C, 1 min; step 2, 95 °C, 30 s; step 3, 45 °C, 30 s; step 4, 72 °C, 1 min; step 5, 72 °C, 10 min; steps 2−4 were repeated 40 times. The amplified DNA was digested with 2.1 units of DNase I at 20 °C for 17 min, which yielded fragments in the size range of 50−200 bp. Without further purification, these fragments were reassembled in a PCR without added primers, again using Taq DNA polymerase. The following conditions were applied: step 1, 95 °C, 1 min; step 2, 95 °C, 30 s; step 3, 40 °C, 30 s; step 4, 72 °C, 1 min; step 5, 72 °C, 10 min; steps 2−4 were repeated 60 times. A final PCR was performed with Taq polymerase, using the reassembled fragments as template and the oligonucleotides 5′-TTAGGATCC*CTGGTTCCGCGT-GGCAGCATG*AACATTAACGAAATTCTGAAAAAACTC-3′ (*Bam*HI restriction site underlined; thrombin/trypsin cleavage site and ATG start codon in italics) and 5′-CCACAAAGCTT-TAGTTTAACCACTACTTTTCA-3′ (*Hin*dIII restriction site underlined) as 5′- and 3′-primers, respectively. The following amplification conditions were used: step 1, 95 °C, 1 min; step 2, 95 °C, 30 s; step 3, 60 °C, 30 s; step 4, 72 °C, 1 min; step 5, 72 °C, 10 min; steps 2−4 were repeated 35 times. The amplified fragments containing the full-length ss*trp*D genes were purified, digested with *Bam*HI and *Hin*dIII, and ligated into the pQE40 vector. Electro-competent DH5α cells were transformed with the ligation mixture, plated on two oversized metal LB agar plates (32 × 38 cm) containing ampicillin, and incubated overnight at 37 °C. The grown cells were harvested from the plates, and the pool of pQE40-ss*trp*D plasmids was isolated. The ss*trp*D gene library contained about $10^6$ independent clones, as estimated from the number of colonies that appeared on an LB agar plate on which a small volume of highly diluted transformants was streaked.

*Selection of ssAnPRT Mutants with Improved Catalytic Activity*. Selection for ssAnPRT mutants with increased catalytic activity was performed with the help of the *E. coli* strain JMB9 ($r^-m^+leu^-b^-$ Δ*trp* LD102) (*34*). This strain is termed Δ*trp*EGD here, because it lacks the first three genes of the tryptophan biosynthetic pathway, which code for the anthranilate synthase (TrpEG complex) and the anthranilate phosphoribosyltransferase (TrpD = AnPRT). For growth on medium without tryptophan, Δ*trp*EGD requires supplementation with anthranilate and transformation with a functional *trp*D gene. Electrocompetent Δ*trp*EGD cells were transformed with 3 μg of the pQE40-ss*trp*D plasmid gene library, incubated in LB medium for 1 h at 37 °C, and washed three times with 1% NaCl. The cells were plated on Vogel−Bonner (VB) medium (*35*) containing 150 μg/mL ampicillin, 10 μg/mL anthranilate, 0.5% casamino acids, 0.2% glucose, 10 μM $FeCl_3$, and 2 μg/mL thiamin and incubated at 37 °C until visible colonies appeared.

*Site-Directed Mutagenesis*. Point mutations were introduced into the ss*trp*D gene by overlap extension PCR (*36*, *37*) using the plasmid pQE40-ss*trp*D (*31*) as template. For the generation of megaprimers by PCR reactions, the oligonucleotides CyRI (*33*) and 5′- ACAGGTGGCGGCGGATTAGGG-3′ (for construction of ss*trp*D-D83G) or 5′-TTCGTTTTCCTC-TCTGCACAATACTAT-3′ (for construction of ss*trp*D-F149S) were used as 5′-primers, and the oligonucleotides Cy*Pst*I (*33*) and 5′-CCCTAATCCGCCGCCACCTGT-3′ (for construction of ss*trp*D-D83G) or 5′-ATAGTATTGTGCAGAGAGGAAA-ACGAA-3′ (for construction of ss*trp*D-F149S) were used as 3′-primers (new codons are underlined). The megaprimers were purified and used in a third PCR reaction, together with CyRI and Cy*Pst*I. The resulting full-length products were digested with *Bam*HI and *Hin*dIII and ligated into pQE40.

*Heterologous Expression of sstrpD Genes and Purification of Recombinant ssAnPRT Proteins*. Wild-type ssAnPRT protein and its mutants were expressed heterologously at 37 °C in *E. coli* strain W3110 *trp*EA2, containing the helper plasmid pDM,1 (*33*). The resulting recombinant protein products were purified from the soluble fraction of the crude extract by heat precipitation of the host proteins and metal chelate affinity chromatography. Details of gene expression and protein purification were similar to our previous studies (*26*). The purity of the recombinant proteins as judged from SDS−PAGE was >95%, and the yields were 0.4−0.8 mg of protein/1 g of wet cell mass. The proteins were dropped into liquid nitrogen and stored at −80 °C. Enzyme concentrations were determined by measuring the absorbance at 280 nm, using a molar extinction coefficient for the monomer of 11920 $M^{-1}$ $cm^{-1}$ as calculated from the amino acid sequence (*38*).

*Steady-State Enzyme Kinetics*. The ssAnPRT reaction was followed at 37 °C by a fluorometric assay performed in 50 mM Tris-HCl, pH 7.2, and the indicated concentration of $MgCl_2$ (*31*), using a CARY Eclipse fluorescence spectrophotometer (Varian). In order to prevent product inhibition, a molar excess of PRA isomerase (TrpF) and indole-3-glycerol phosphate synthase (TrpC) from *T. maritima* were added. The Michaelis constants ($K_M^{AA}$ and $K_M^{PRPP}$) were determined by fitting a hyperbolic equation (program SigmaPlot) to the saturation curves that were constructed on the basis of initial velocity measurements recorded in the presence of an excess ($10K_M$) of the second substrate. The turnover number ($k_{cat}$) was obtained by dividing the fitted maximum catalytic rate ($V_{max}$) by the concentration of active sites ($[E_o]$).

*Analysis of the PRPP and $Mg^{2+}$ Dependence of Initial Turnover Rates*. Initial turnover rates of ssAnPRT were recorded for different concentrations of $MgCl_2$ and PRPP in the presence of saturating concentrations of AA. The following ligand binding model was fitted to the experimental data sets: it comprises the equilibrium equations for the formation of the substrate Mg·PRPP in solution ($K_D1$) and binding of Mg·PRPP to ssAnPRT·AA ($K_D2$). (Since the order of substrate binding is not known, we cannot distinguish whether Mg·PRPP actually binds to the preformed ssAnPRT·AA complex or rather to ssAnPRT, followed by AA binding. However, this is irrelevant for our analysis.) Binding of free $Mg^{2+}$ to ssAnPRT·AA·Mg·PRPP yields the ssAnPRT·AA·$Mg_2$·PRPP complex ($K_D3$):

$$Mg^{2+} + PRPP^{5-} \rightleftharpoons Mg\cdot PRPP^{3-} \quad (K_D1)$$

$$ssAnPRT\cdot AA + Mg\cdot PRPP^{3-} \rightleftharpoons ssAnPRT\cdot AA\cdot Mg\cdot PRPP^{3-} \quad (K_D2)$$

$$ssAnPRT\cdot AA\cdot Mg\cdot PRPP^{3-} + Mg^{2+} \rightleftharpoons ssAnPRT\cdot AA\cdot Mg_2\cdot PRPP^{1-} \quad (K_D3)$$

For fitting the model to experimental data sets the program DynaFit (BioKin Ltd.) (*39*) was applied, which computes the composition of complex mixtures at equilibrium by simultaneously solving the mass balance equation for the component species using the multidimensional Newton−Raphson method. $K_D1$, the dissociation constant for the formation of Mg·PRPP in solution, was fixed in the simulation to 0.59 mM (*40*), whereas the dissociation constants $K_D2$ and $K_D3$ and the response coefficient associated with ssAnPRT·AA·Mg·PRPP were optimized in the fit (Supporting Information Table S2). Our presumption is that the concentration of the ssAnPRT·AA·Mg·PRPP complex is directly proportional to the experimentally determined initial turnover rates, whereas the ssAnPRT·AA·$Mg_2$·PRPP complex is unproductive. The analysis was conducted assuming that the PRPP stock solution contains traces of Mg·PRPP, the exact value (0.9%) also being optimized in the fitting procedure. Both for ssAnPRT-wt and ssAnPRT-D83G + F149S, two data sets (1, variable amount of PRPP at constant concentration of $MgCl_2$; 2, variable amount of $MgCl_2$ at constant concentration of PRPP) were analyzed independently, and therefore two sets of estimated parameters were obtained. They are shown in Supporting Information Table S2, together with their 99% confidence intervals.

*Transient Kinetics*. The experiments were performed using a SX20 stopped-flow reaction analyzer (Applied Photophysics) thermostated at 37 °C. All given concentrations refer to final concentrations in the observation cell. Progress curves were determined in 50 mM Tris-HCl, pH 7.2, by monitoring changes of fluorescence (excitation wavelength 313 nm; emission cutoff filter 395 nm), and the results of at least five mixing experiments were averaged. Each set of presented data is representative of at least two independent series of measurements performed with different protein batches. An exponential equation [$y = a \exp(-k_{obs}t)$ + offset, program SigmaPlot] was fitted to the data. The fitted $k_{obs}$ values were replotted as a function of the ssAnPRT concentration. The maximum rate, which corresponds to $k_{trans}$ in Figure 1A, was estimated by fitting the following equation to these data:

$$k_{obs} = \text{ssAnPRT} \times k_{trans}/(\text{ssAnPRT} + K_S)$$

whereby $K_s$ is the apparent binding constant for anthranilate to ssAnPRT.

*Thermal Denaturation*. Thermal denaturation was monitored by circular dichroism in a 0.1 cm cuvette, following the change in ellipticity at 220 nm in a JASCO J-815 CD spectrometer. The enzyme at a concentration of 10 $\mu$M in 10 mM potassium phosphate, pH 7.5, was unfolded by raising the temperature in 0.1 °C increments at a ramp rate of 1 °C/min using a Peltier effect temperature controller. Unfolding was irreversible, due to protein aggregation and precipitation. Measured ellipticity was normalized, and the midpoint temperature of the unfolding transition ($T_m$) was determined. Kinetics of irreversible heat inactivation were measured similar to our previous studies (*30*). Shortly, the proteins were incubated at 80 °C in 50 mM Tris-HCl, pH 6.5, assuming a $\Delta pK_a$/°C for Tris buffer of −0.028 (*41*). Aliquots were taken at different times, chilled on ice, and centrifuged. The residual enzymatic activity of ssAnPRT in the supernatant was measured at 37 °C in 50 mM Tris-HCl, pH 7.7.

*Crystal Structure Elucidation*. Crystals were obtained by the hanging drop, vapor diffusion method in 24-well VDX plates (Hampton Research) at 20 °C. Drops consisted of 1 $\mu$L:1 $\mu$L mixtures of protein and reservoir solutions, where the reservoir contained 18% PEG 1500 (w/v), 10% glycerol (v/v), and 50 mM MES, pH 6.0, and the protein solution consisted of ssAnPRT-D83G + F149S concentrated to 5 mg/mL in 10 mM HEPES, pH 8.0. Crystals grew as thin plates within 3 days. For substrate complexation in the crystalline state, single crystals of the apoenzyme were immersed in mother liquor supplemented with 2.5 mM PRPP and 1.25 mM $MnCl_2$ for 60 min. The long soaking times were required to allow for lattice reannealing since crystals underwent visible deterioration upon initial contact with the ligands. The crystals were then briefly transferred to a cryosolution composed of soaking medium supplemented with 20% glycerol (v/v) and rapidly flash frozen in liquid nitrogen. X-ray diffraction data were collected from a single crystal at 100 K on beamline X06SA, SLS, Villigen. Data processing used the XDS/XSCALE suite (*42*), and phasing was by molecular replacement in PHASER (*43*), using the crystal structure of wild-type ssAnPRT (PDB entry 1ZYK) in its apo form as search model. Inspection of electron density maps, manual model building, and refinement were carried out in Refmac5 (*44*) and Coot (*45*) until free and crystallographic *R*-factors could not be lowered any further. For cross-validation during refinement, diffraction data were divided into a working and a test set using FREERFLAG (*46*). The model for the PRPP substrate was created and refined using CCP4 libraries. To avoid model bias PRPP and $Mn^{2+}$ ions were added to the structure only in the latest stages of refinement. X-ray data collection and structure refinement statistics are given in Supporting Information Table S3, and coordination distances between PRPP and metals are given in Supporting Information Table S4. Stereo representations of ligands bound to ssAnPRT-D83G + F149S and their corresponding unambiguous electron density maps are shown in Supporting Information Figure S1.

## RESULTS

*Isolation of Activated ssAnPRT Mutants by Library Selection*. The *E. coli* strain Δ*trp*EGD, which lacks chromosomal genes copies for anthranilate synthase (TrpEG complex) and anthranilate phosphoribosyltransferase (TrpD), was transformed with an ss*trp*D plasmid library generated by DNA shuffling (*32*). The method produces a point mutagenesis rate of 0.7%, similar to error-prone PCR (*47*). The transformants were plated on minimal agar supplemented with anthranilate, in order to substitute for the lacking TrpEG complex, and incubated at 37 °C. Whereas Δ*trp*EGD cells transformed with the wild-type ss*trp*D gene formed visible colonies after more than 80 h, a number of cells transformed with the ss*trp*D gene library grew to a visible size within 16−48 h.

The faster growing colonies were assumed to produce ssAnPRT mutants with a higher catalytic activity than the wild-type enzyme at 37 °C, which is more than 40 °C below the physiological temperature of *S. solfataricus* (*48*). From the seven fastest growing colonies, plasmid was isolated, and the ss*trp*D inserts were sequenced. Three of the seven inserts contained identical mutations. Each of the remaining five different ss*trp*D genes coded for several amino acid exchanges and additionally contained a varying number of silent mutations (Supporting Information Table S1). All but one of the isolated ssAnPRT mutant proteins carried the exchanges of both aspartate 83 by glycine (D83G) or asparagine (D83N) and phenylalanine 149 by serine (F149S). In order to quantify the increase in enzymatic activity caused by these mutations, the

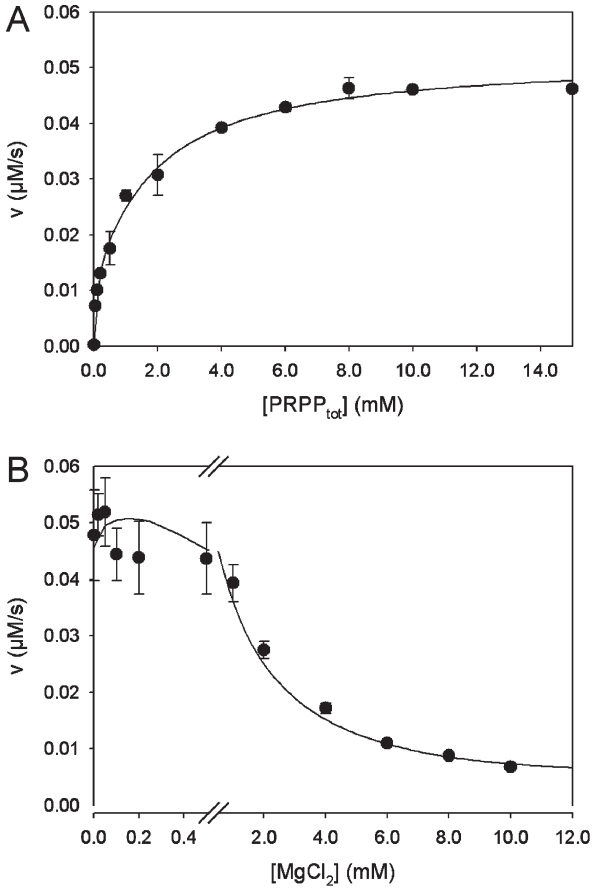


FIGURE 2: [PRPP$_{tot}$] and [MgCl$_2$] dependence of the steady-state activity of ssAnPRT-wt. Initial velocities of the turnover of 5 $\mu$M AA by 0.25 $\mu$M ssAnPRT-wt were measured at 37 °C in 50 mM Tris-HCl, pH 7.2, (A) in the presence of 0.5 mM MgCl$_2$ while varying [PRPP$_{tot}$] and (B) in the presence of 10 mM PRPP while varying [MgCl$_2$]. Circles (●) correspond to experimentally measured values, and error bars indicate the standard deviation observed in at least two separate experiments. Solid lines represent the best fit with equilibrium equations of the ligand binding model outlined in the Experimental Procedures.

ssAnPRT-D83G + F149S protein was overproduced in *E. coli* and purified from the soluble fraction of the cell extract. Moreover, in order to evaluate the effect of the individual residue exchanges, the ssAnPRT-D83G and ssAnPRT-F149S single mutants were generated by site-directed mutagenesis, and the recombinant proteins were also produced and purified. The association states of the three mutants were investigated by gel filtration chromatography on a calibrated Superdex 75 column. The measured elution times were compatible with a dimeric association state, as observed for the ssAnPRT-wt enzyme (*31*).

*Magnesium Dependence of Catalytic Activity*. We previously observed that the catalytic activity of wild-type ssAnPRT is inhibited by high concentrations of $Mg^{2+}$ (*26*). In order to test whether this inhibition has been removed in the selected double mutant, the initial velocities of substrate turnover by ssAnPRT-wt and ssAnPRT-D83G + F149S were measured by fluorescence spectroscopy at 37 °C. Thereby the anthranilate and enzyme concentrations were held constant while varying the concentration of PRPP at a fixed concentration of MgCl$_2$ or varying the concentration of MgCl$_2$ at a fixed concentration of PRPP. The PRPP and MgCl$_2$ dependencies of the initial velocities are shown in Figure 2 for ssAnPRT-wt and in Figure 3 for ssAnPRT-D83G + F149S.

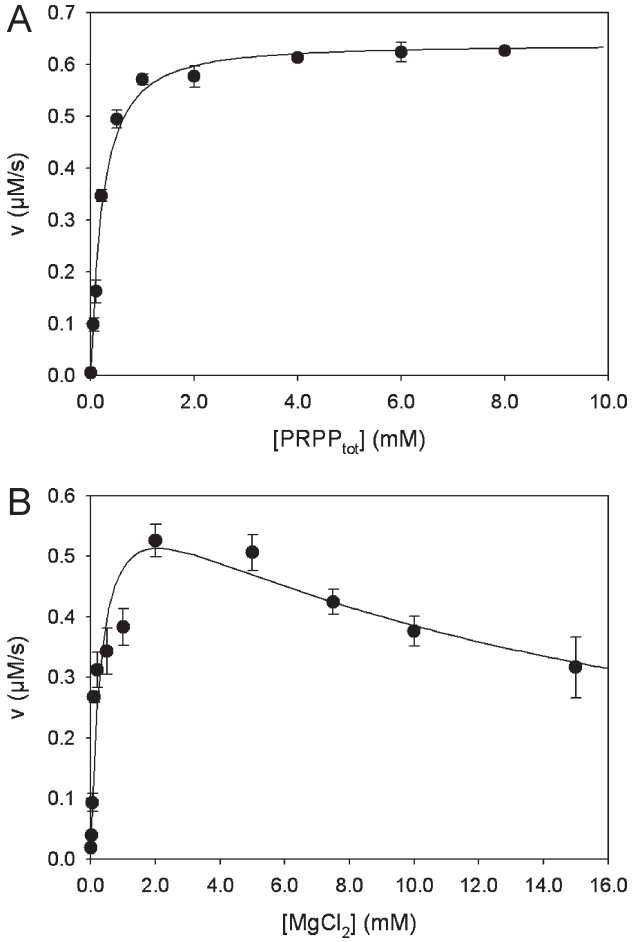


FIGURE 3: [PRPP$_{tot}$] and [MgCl$_2$] dependence of the steady-state activity of ssAnPRT-D83G + F149S. Initial velocities of the turnover of 30 $\mu$M AA by 0.10 $\mu$M ssAnPRT-D83G + F149S were measured at 37 °C in 50 mM Tris-HCl, pH 7.2, (A) in the presence of 1 mM MgCl$_2$ while varying [PRPP$_{tot}$] and (B) in the presence of 1 mM PRPP while varying [MgCl$_2$]. Circles (●) correspond to experimentally measured values, and error bars indicate the standard deviation observed in at least two separate experiments. Solid lines represent the best fit to equilibrium equations of the ligand binding model outlined in the Experimental Procedures.

In accordance with expectation the initial reaction rate increased with increasing concentrations of PRPP, both for ssAnPRT-wt (Figure 2A) and ssAnPRT-D83G + F149S (Figure 3A). However, for ssAnPRT-wt a marked inhibition of the activity was observed at MgCl$_2$ concentrations higher than 0.1 mM (Figure 2B). In contrast, the activity of ssAnPRT-D83G + F149S increased up to about 2−5 mM MgCl$_2$ and decreased only moderately at higher $Mg^{2+}$ concentrations (Figure 3B). While the single mutant ssAnPRT-F149S was inhibited by MgCl$_2$ to a similar extent as ssAnPRT-wt, the initial reaction rate of the single mutant ssAnPRT-D83G was decreased only at very high concentrations of MgCl$_2$ (data not shown), as observed for ssAnPRT-D83G + F149S.

*Crystal Structure Analysis and Modeling of Inhibition by High $Mg^{2+}$ Concentrations*. The X-ray structure of ssAnPRT-wt in complex with substrates (*26*) showed that each of the two protomers of the dimer binds two molecules of anthranilate, one molecule of PRPP, and two $Mg^{2+}$ ions or two equivalent $Mn^{2+}$ ions (Figure 1B,C). The high-affinity metal-binding site (Mg-I) is defined by interactions of $Mg^{2+}$ with ribose and pyrophosphate oxygen atoms of PRPP, without any direct contacts to the protein. The low-affinity metal-binding

site (Mg-II) is formed by the 5′-phosphate moiety of PRPP and the negatively charged protein residues aspartate 223 (D223) and glutamate 224 (E224). Whereas the Mg-I binding site is common in all classes of PRTs, the Mg-II site is specific for AnPRTs, where D223 and E224 are conserved.

We have solved the crystal structure of ssAnPRT-D83G + F149S in complex with PRPP and $Mn^{2+}$ ions, which can be identified more reliably in electron density maps than $Mg^{2+}$, to 2.25 Å resolution. The observed crystal form contains a biological dimer in its asymmetric unit, with both protomers exhibiting identical protein conformations and ligand coordination sites. Moreover, the protein backbone of ssAnPRT-D83G + F149S shows no detectable differences to the wild-type enzyme, proving that the mutations do not alter the overall conformation. The data reveal, however, that PRPP bound to ssAnPRT-D83G + F149S adopts an extended conformation that contrasts markedly with the "S" compact shape observed in complexes of the wild-type enzyme (*26*) (Figure 1C). The extended PRPP conformation resembles but is not identical to the one observed in AnPRT from *M. tuberculosis* (mtAnPRT) (*29*). The altered binding mode of PRPP causes this substrate to span into the N-terminal α-helical domain of the double mutant, approaching the binding sites for anthranilate.

It appears that the "S" shape of PRPP in ssAnPRT-wt is stabilized by a hydrogen bond between the 5′-phosphate group of the substrate and the carboxyl side chain of aspartate 83 (*26*), which requires that one of the two acidic groups is protonated. Although an equivalent aspartate residue is present in mtAnPRT (Figure 1C), its p$K_a$ value or that of the 5′-phosphate group of the bound ligand might be too low to allow for hydrogen bond formation. Within ssAnPRT-D83G + F149S, the hydrogen bond is lost as a result of the D83G exchange. For wild-type ssAnPRT, the 5′-phosphate group of PRPP is involved in the binding of the Mg-II ion (*26*). Although a bivalent cation is also present at related locations in mtAnPRT and ssAnPRT-D83G + F149S, the 5′-phosphate group of the extended PRPP is too far apart to contribute to its binding (Figure 1C). We therefore speculated that the affinity of Mg-II for the active site might be decreased and thus the propensity for the formation of a putatively inhibitory $Mg_2$·PRPP complex might be lower in ssAnPRT-D83G + F149S than in wild-type ssAnPRT.

In order to test this hypothesis, we formulated a corresponding binding model and applied nonlinear least-squares fitting to obtain the parameters from the PRPP and $MgCl_2$ dependencies of ssAnPRT-wt (Figure 2) and ssAnPRT-D83G + F149S (Figure 3). The model permits formation of Mg·PRPP in solution ($K_D$1 = 0.59 mM) (*40*), followed by its binding to ssAnPRT·AA ($K_D$2) and turnover. Binding of free $Mg^{2+}$ to the ssAnPRT·AA·Mg·PRPP complex ($K_D$3) results in the formation of an unproductive ssAnPRT·AA·$Mg_2$·PRPP complex which is not turned over, accounting for the inhibitory effect of high concentrations of $Mg^{2+}$. In solution PRPP forms a predominant monomagnesium complex; it also can form dimagnesium complexes in metal-rich media, but with very low affinity ($K_D$ = 21.3 mM) (*40*, *49*). Moreover, the 5′-phosphate group of PRPP is involved in the binding of Mg-II in ssAnPRT-wt but not in the activated double mutant (Figure 1C). For these reasons, we used a model where the second $Mg^{2+}$ ion associates with the enzyme-bound but not with the free Mg·PRPP complex, instead of an alternative model which would permit direct binding of $Mg_2$·PRPP to the active site.

Both data sets, with fixed concentration of $MgCl_2$ (Figures 2A and 3A) or fixed concentration of PRPP (Figures 2B and 3B), were analyzed independently. Nevertheless, the model returned consistent parameter estimates of the equilibrium constants for both data sets (Supporting Information Table S2). For wild-type ssAnPRT the fitting analysis yielded $K_D$2 values of 50 and 150 μM, whereas $K_D$2 values of 150 and 240 μM were calculated for ssAnPRT-D83 + F149S. These results indicate that the Mg·PRPP substrate binds with similar affinity to the wild-type and the double mutant enzyme. However, the fitted $K_D$3 values of 60 and 190 μM for ssAnPRT-wt are lower by about 2 orders of magnitude than the $K_D$3 values of 14 and > 30 mM that were determined for ssAnPRT-D83G + F149S, indicating that the affinity of free $Mg^{2+}$ for enzyme-bound Mg·PRPP is much lower in the double mutant. As a consequence, the capacity to form the inhibitory ssAnPRT·AA·$Mg_2$·PRPP complex is reduced significantly in the activated variant, as suggested from crystal structure analysis.

Table 1: Steady-State Enzyme Kinetic Constants of Wild-Type ssAnPRT and the Activated Mutants[a]

| ssAnPRT protein | $MgCl_2$ (μM) | $K_M^{AA}$ (μM) | $K_M^{PRPP}$ (μM) | $k_{cat}$ ($s^{-1}$) | $k_{cat}^{var}/k_{cat}^{wt}$ [b] |
|---|---|---|---|---|---|
| wild type | 50 | 0.018 | 47 | 0.33 | |
| wild type | 2000 | 0.020 | 1540 | 0.24 | |
| D83G + F149S | 50 | 3.6 | 13 | 4.4 | 13.3 |
| D83G + F149S | 2000 | 3.1 | 23 | 13.3 | 40.3 |
| D83G | 2000 | 0.12 | 38 | 2 | 6.1 |
| F149S | 50 | 1.2 | 151 | 1.2 | 3.6 |

[a] The steady-state constants were determined from saturation curves, which were constructed from initial velocities measured at different concentrations of AA and PRPP, in the presence of saturating concentrations of the second substrate (> 10$K_M$). The measurements were performed in 50 mM Tris-HCl, pH 7.2 at 37 °C, in the presence of the given concentrations of $MgCl_2$. The values are the averages of two experiments, and standard errors are less than 10%. [b] $k_{cat}$ values measured at the respective optimum concentrations of $MgCl_2$ were compared.

*Michaelis Constants and Turnover Numbers*. Saturation curves for anthranilate and PRPP, in the presence of an excess of the second substrate, were monitored for wild-type ssAnPRT, the ssAnPRT-D83G + F149S double mutant, and the two single mutants. The deduced Michaelis constants and turnover numbers in the presence of different concentrations of $MgCl_2$ are listed in Table 1. For wild-type ssAnPRT, the value of the Michaelis constant for PRPP reached its minimum at 50 μM $MgCl_2$ and was about 30-fold higher at 2 mM $MgCl_2$, in accordance with the observed inhibition of catalytic activity at high concentrations of $MgCl_2$ (Figure 2B). The turnover number ($k_{cat}$) for ssAnPRT-wt was much less affected by the $MgCl_2$ concentration, both at 37 °C (Table 1) and at 60 °C (*26*). These data suggest that $Mg_2$·PRPP acts as a competitive inhibitior of the binding of Mg·PRPP to wild-type ssAnPRT, in accordance with the model outlined in the previous paragraph. In contrast, for ssAnPRT-D83G + F149S, the $K_M^{PRPP}$ values at 50 μM and 2 mM $MgCl_2$ are practically identical (Table 1). Remarkably, the $K_M^{AA}$ value of the double mutant is drastically increased compared to the wild-type enzyme, irrespective of the $MgCl_2$ concentration. Obviously, there was no selective pressure for the ssAnPRT variants to maintain the low $K_M^{AA}$ of the wild-type enzyme, presumably because high concentrations of this substrate (10 μg/mL = 73 μM) were present on the agar plates. When determined at the respective optimum $MgCl_2$ concentration, the $K_M^{PRPP}$ values of the ssAnPRT-D83G + F149S double mutant and the two single mutants are of the same order of magnitude as for the wild-type enzyme, whereas the $k_{cat}$ value is

increased 40-fold for the double mutant and 6-fold and 4-fold, respectively, for ssAnPRT-D83G and ssAnPRT-F149S. As a consequence, the catalytic efficiency parameter $k_{cat}/K_M^{AA}$ of all variants is lowered with respect to the wild-type enzyme, whereas $k_{cat}/K_M^{PRPP}$ of ssAnPRT-D83G and ssAnPRT-D83G + F149S is increased by 2 orders of magnitude.

*Rate-Limiting Step of the Reaction*. A minimal catalytic mechanism of the reaction catalyzed by anthranilate phosphoribosyltransferase is presented in Figure 1A. Whereas studies on AnPRT from *Saccharomyces cerevisiae* suggest that anthranilate and PRPP bind in a random order sequential fashion (*50*), we cannot exclude that a compulsory binding mechanism is effective in ssAnPRT. In any case, after formation of the ternary ssAnPRT·AA·PRPP complex, a phosphoribosyl moiety is transferred from PRPP to AA (described by $k_{trans}$), followed by the release of the products $PP_i$ and PRA (described by $k_{off}$). The double mutation D83G + F149S results in an increase of the turnover number at 37 °C by a factor of about 40 when measured at the respective optimum $MgCl_2$ concentration (Table 1). The turnover number obtained from the steady-state kinetic data depends on both the chemical transfer and the product release step: $k_{cat} = (k_{trans}k_{off})/(k_{trans} + k_{off})$. Therefore, the increase in $k_{cat}$ observed for the double mutant could be caused by an increase of either $k_{trans}$ or $k_{off}$, depending on whether the irreversible chemical transfer is rate-limiting and product release is comparably fast ($k_{trans} < k_{off}$), or vice versa ($k_{trans} > k_{off}$).

To distinguish between the two possibilities, the turnover numbers of wild-type ssAnPRT and ssAnPRT-D83G + F149S determined by steady-state kinetics were compared with the value of $k_{trans}$ as determined from transient kinetic experiments in a stopped-flow apparatus. To this end, a preincubated solution containing AA and an excess of ssAnPRT was rapidly mixed with saturating concentrations of PRPP in the presence of the respective optimal concentration of $MgCl_2$. Under conditions where the formation of ssAnPRT·AA·PRPP is complete within the dead time of the experiment (ssAnPRT·AA·PRPP $\approx [A]_{total}$, single-turnover conditions), the reaction is described by a two-step irreversible process (Figure 1A). Since the spectroscopic change occurs at the transition from ssAnPRT·AA·PRPP to ssAnPRT·PRA·$PP_i$, the observed first-order rate constant corresponds to $k_{trans}$. This conclusion is independent of whether the two substrates bind with a random or a compulsory mechanism as long as single-turnover conditions are met. The conversion of AA to PRA by ssAnPRT-D83G + F149S in the presence of 2 mM $MgCl_2$ is shown in Figure 4A, and the corresponding observed first-order rate constants are plotted as a function of the enzyme concentration in Figure 4C. Fitting a hyperbolic curve to the data yielded a limiting value of $k_{trans} = 29.6 \pm 0.9\ s^{-1}$ (*51*, *52*). (The interpretation of the shape of the hyperbola will depend on the substrate binding mechanism, which is unknown at present.) The $k_{cat}$ value determined in a steady-state kinetic experiment under identical conditions was $13.3 \pm 1.1\ s^{-1}$ (Table 1). From the relationship $k_{cat} = (k_{trans}k_{off})/(k_{trans} + k_{off})$, it follows that $k_{off} = (k_{cat}k_{trans})/(k_{trans} - k_{cat}) = 24.2 \pm 2.0\ s^{-1}$ (Table 2). Since $k_{trans}$ and $k_{off}$ are of the same order of magnitude, phosphoribosyl transfer and product release affect catalytic turnover equally. When monitoring the enzymatic reaction of ssAnPRT-wt in the presence of 50 $\mu$M $MgCl_2$, we observed deviations from first-order kinetics (Figure 4B). In order to get an estimate for the limiting value, we nevertheless plotted the observed rate constants as a function of the ssAnPRT-wt concentration (Figure 4D). The hyperbolic fit yielded a $k_{trans}$ value of $3.3 \pm 0.16\ s^{-1}$ (Table 2), but the actual value might be higher since the measured curves are somewhat steeper than the curves obtained from fitting a simple monoexponential equation to the data. The $k_{cat}$ value determined in steady-state measurements under identical conditions was $0.33 \pm 0.02\ s^{-1}$ (Table 1). Irrespective of the exact value of $k_{trans}$ the relationship $k_{cat} = (k_{trans}k_{off})/(k_{trans} + k_{off})$ implies that the values of $k_{off}$ and $k_{cat}$ will be very similar (Table 2), demonstrating that product release is the rate-limiting step in the catalytic cycle of ssAnPRT-wt ($k_{off} < k_{trans}$). In summary, the comparison of steady-state and single-turnover data shows that the increased turnover number of ssAnPRT-D83G + F149S is mainly based on an acceleration of PRA release.

*Thermal Stability*. The thermal stabilities of wild-type ssAnPRT and the activated mutants were determined by heat denaturation which was monitored using far-UV circular dichroism spectroscopy (Figure 5A). Since thermal denaturation was irreversible, we used the apparent melting temperatures ($T_m$) as an operational measure to assess the effects of the mutations on conformational stability. The ssAnPRT-wt protein and ssAnPRT-D83G showed $T_m$ values of 90 and 91 °C, respectively, whereas the ssAnPRT-F149S protein and the double mutant exhibited $T_m$ values of 82 °C (Table 3). These data show that the D83G exchange is neutral in terms of stability, whereas the F149S exchange is destabilizing.

Furthermore, the kinetics of irreversible heat inactivation was monitored for ssAnPRT-wt and the activated variants. For that purpose the enzymes were incubated at 80 °C, and residual activities of samples withdrawn after different time intervals were measured at 37 °C. For all ssAnPRT variants, the decay of enzymatic activity as a function of time was an first-order process, which allowed us to determine apparent half-lives ($t^{app}_{1/2}$) as an operational measure of kinetic stability (Figure 5B, Table 3). In accordance with the observed $T_m$ values, ssAnPRT-D83G ($t^{app}_{1/2}$ = 77 min) resembles ssAnPRT-wt ($t^{app}_{1/2}$ = 60 min), whereas ssAnPRT-F149S ($t^{app}_{1/2}$ = 6.0 min) and ssAnPRT-D83G + F149S ($t^{app}_{1/2}$ = 4.1 min) lose catalytic activity much more rapidly.

## DISCUSSION

We have isolated from an ss*trp*D gene library the activated double mutant ssAnPRT-D83G + F149S. The crystal structure of ssAnPRT-wt (*26*) shows that aspartate 83 is part of the $^{79}$GTGGD$^{83}$ loop, which becomes structured upon binding of PRPP. The second position relevant for activation, phenylalanine 149, is located adjacent to alanine 150, which is part of the binding pocket for AA-I (Figure 1B). *In vitro* characterization of wild-type ssAnPRT and the activated double mutant demonstrated that the amino acid exchanges have two main consequences for the enzymatic activity of ssAnPRT, namely, abolition of inhibition by high $Mg^{2+}$ concentrations and accelerated release of the product PRA from the active site.

*Removal of Mg Inhibition*. A marked inhibition of the reaction catalyzed by wild-type ssAnPRT was observed at $MgCl_2$ concentrations higher than 0.1 mM, whereas no significant inhibitory effect on ssAnPRT-D83G + F149S was measurable up to concentrations of 5 mM $MgCl_2$ (Figures 2B and 3B). We have attributed this difference to a higher propensity for ssAnPRT-wt to form the unproductive $Mg_2$·PRPP complex, which is not turned over but competes with the true substrate Mg·PRPP for the PRPP binding site on the enzyme. This binding mechanism does establish the simplest model that is qualitatively

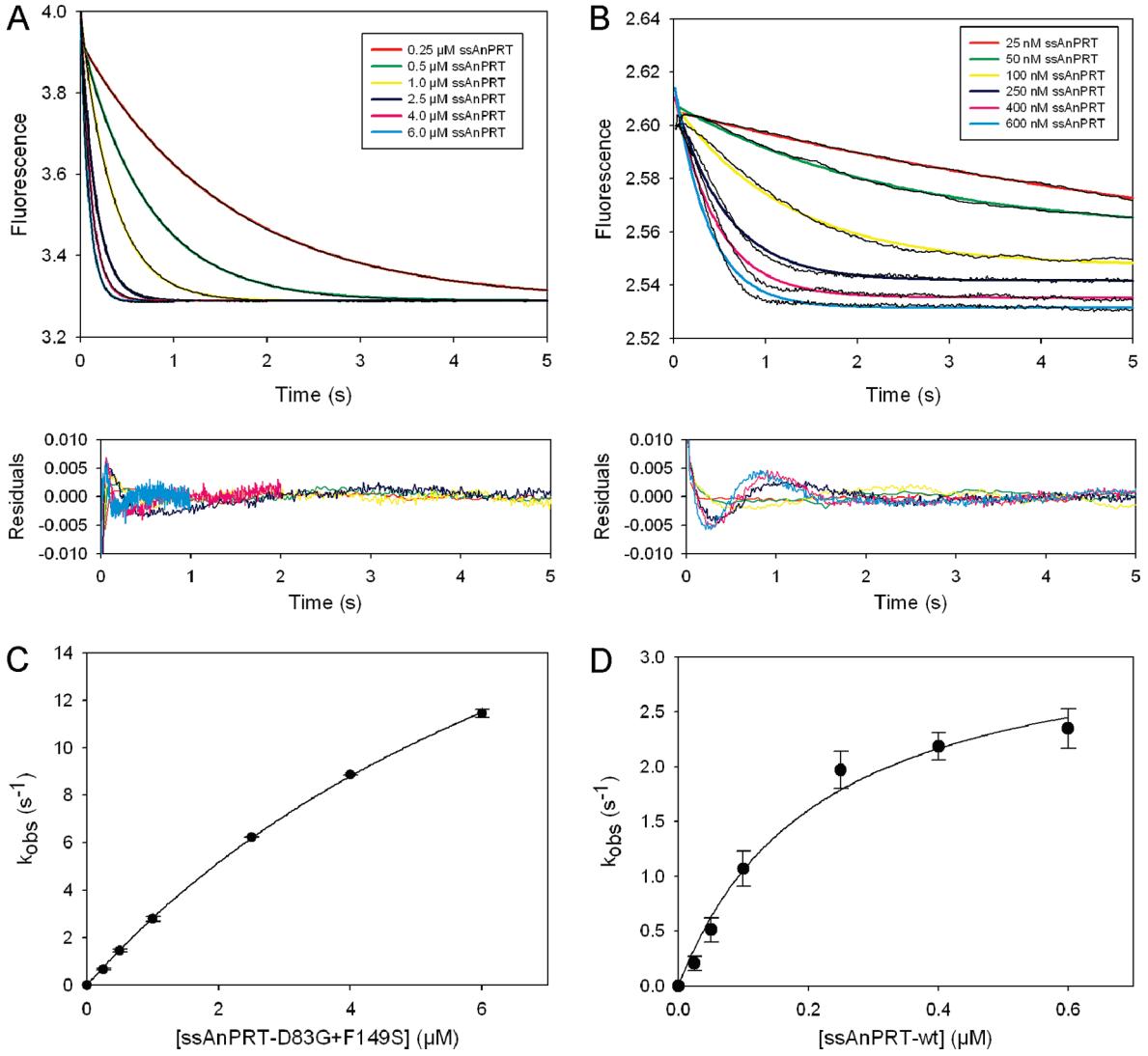


FIGURE 4: Transient kinetic analysis of (A, C) ssAnPRT-D83G + F149S and (B, D) ssAnPRT-wt. Solutions containing the indicated concentrations of (A) ssAnPRT-D83G + F149S and 0.1 $\mu$M AA or (B) ssAnPRT-wt and 0.01 $\mu$M AA were rapidly mixed with a solution containing 1 mM PRPP (concentrations are cell concentrations), and the turnover to PRA was monitored by recording the fluorescence decrease. A monoexponential equation reflecting a first-order rate mechanism was fitted to the data (data, black line; fit, colored lines). The bottom graphs show the deviation between data and fit. (C) Fitted exponential decay rates were plotted as a function of ssAnPRT-D83G + F149S concentration. The hyperbolic fit (black sold line) yielded $k_{trans} = 29.6 \pm 0.9\ s^{-1}$. (D) Fitted exponential decay rates were plotted as a function of ssAnPRT-wt concentration. The hyperbolic fit (black solid line) yielded $k_{trans} = 3.3 \pm 0.16\ s^{-1}$. Error bars indicate the standard deviation observed in two separate experiments. Measurements were performed at 37 °C in 50 mM Tris-HCl, pH 7.5, and 2 mM $MgCl_2$ for ssAnPRT-D83G + F149S and in 50 $\mu$M $MgCl_2$ for ssAnPRT-wt. (Transients of ssAnPRT-wt monitored in the presence of 2 mM $MgCl_2$ were qualitatively similar but yielded lower $k_{obs}$ values; data not shown.)

Table 2: Rate Constants of Wild-Type ssAnPRT and the Activated Double Mutant[a]

| ssAnPRT protein | $k_{trans}$ ($s^{-1}$) | $k_{off}$ ($s^{-1}$) | $k_{cat}$ ($s^{-1}$) |
|---|---|---|---|
| wild type | > 3.3 | ~0.33 | 0.33 ± 0.02 |
| D83G + F149S | 29.6 ± 0.9 | 24.2 ± 2.0 | 13.3 ± 1.1 |

[a] The measurements were performed in 50 mM Tris-HCl, pH 7.2 at 37 °C, in the presence of 50 $\mu$M $MgCl_2$ (wild type) and 2 mM $MgCl_2$ (D83G + F149S).

consistent with the steady-state enzyme kinetic data and the crystal structures of wild-type and mutant ssAnPRTs.

Selection of activated ssAnPRT variants was conducted with Δ*trp*EGD *E. coli* cells grown on Vogel−Bonner medium, which contains 0.8 mM $Mg_2SO_4$. Since in this concentration range the intracellular concentration of unbound magnesium in *E. coli* cells is the same as the external concentration (*53*), ssAnPRT-D83G + F149S was selected in the presence of 0.8 mM $Mg^{2+}$. Activity of ssAnPRT-wt is reduced at this $Mg^{2+}$ concentration, due to the binding of $Mg_2$·PRPP and the resulting increase of the apparent $K_M^{PRPP}$ value. We conclude that the double mutant was selected either on the basis of its increased turnover number or its increased $k_{cat}/K_M^{PRPP}$ value caused by the lack of inhibition by high $Mg^{2+}$ concentrations. A similar decrease of catalytic activity with increasing $MgCl_2$ concentration was observed at 60 °C (*26*), which makes it likely that the inhibition is also effective at 80 °C, which is the optimum growth temperature of *S. solfataricus*. However, since the intracellular $Mg^{2+}$ concentration of *S. solfataricus* is unknown, it currently remains unclear whether and to which extent the inhibition is also effective under physiological conditions.

*Acceleration of PRA Release*. A comparison of the results obtained in the transient and steady-state kinetic experiments revealed that the turnover of ssAnPRT-wt at 37 °C is limited by

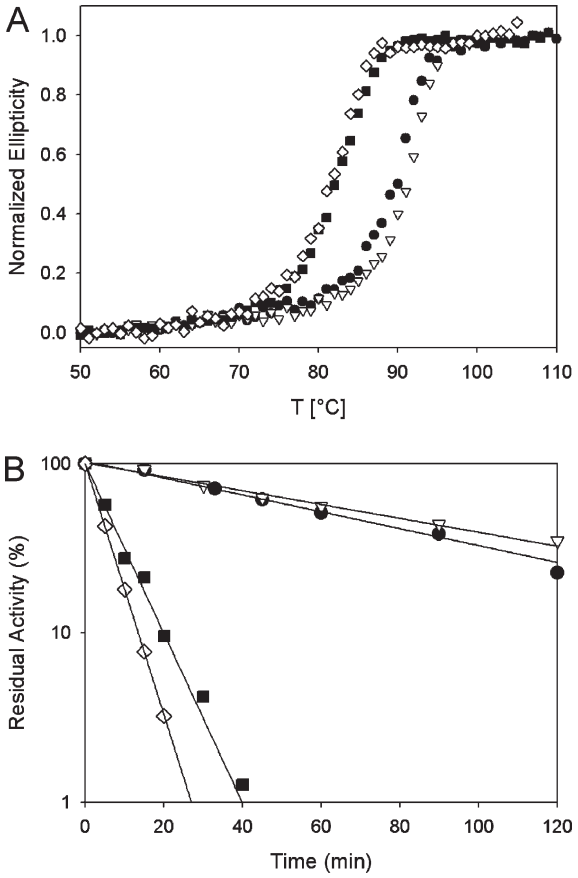


FIGURE 5: Thermal stability of wild-type ssAnPRT and the activated mutants. (A) Thermal denaturation monitored by loss of the far-UV CD signal at 222 nm. The ramp rate was 1 °C/min. Measurements were performed with 10 $\mu$M ssAnPRT in 10 mM potassium phosphate, pH 7.5. (B) Irreversible heat inactivation. Proteins were incubated in 50 mM Tris-HCl, pH 6.5 at 80 °C, and the time-dependent decay of the residual activity was measured at 37 °C. Key: ssAnPRT-wt (●); ssAnPRT-D83G (▽); ssAnPRT-F149S (■); ssAnPRT-D83G + F149S (◇). The values for $T_m$ and $t_{1/2}^{app}$ are shown in Table 3.

Table 3: Unfolding Midpoint Temperatures and Half-Lives of Inactivation of Wild-Type ssAnPRT and the Activated Mutants[a]

| ssAnPRT protein | $T_m$ (°C) | $t_{1/2}^{app}$ at 80 °C (min) |
|---|---|---|
| wild type | 90 | 60 |
| D83G | 91 | 77 |
| F149S | 82 | 6.0 |
| D83G + F149S | 82 | 4.1 |

[a] Thermal denaturation of ssAnPRT was monitored by decrease of the far-UV CD signal at 222 nm in 10 mM potassium phosphate, pH 7.5. For irreversible thermal inactivation proteins were incubated in 50 mM Tris-HCl, pH 6.5 at 80 °C. The $t_{1/2}^{app}$ values were determined from the first-order decay of residual activities at 37 °C.

the dissociation of the enzyme−product complex. Since release of pyrophosphate has been shown to be fast in other PRTases (*54*−*56*) and as we did not observe any product inhibition in the presence of high concentrations of pyrophosphate (data not shown), the slow and rate-limiting step in the enzymatic mechanism of ssAnPRT-wt was attributed to the release of the second product PRA. At 37 °C we measured a forward phosphoribosyl transfer rate of > 3.3 $s^{-1}$, which is at least 10-fold more rapid than the overall rate of forward catalysis (0.33 $s^{-1}$). Rapid on-enzyme phosphoribosyl transfer chemistry with slow product release has previously been reported for various PRTases, for example, human hypoxanthine−guanine (HG) PRTase (*56*) and orotate PRTase (*55*), which possess type I PRTase architecture, and *S. typhimurium* nicotinic acid (NA) PRTase (*54*), which is a type II PRTase (*57*). However, with phosphoribosyl transfer rates of 131 $s^{-1}$ (HG PRTase), 260 $s^{-1}$ (orotate PRTase), and at least 500 $s^{-1}$ (NA PRTase) at 30 °C for the mesophilic PRTases the chemical transfer step proceeds far more rapidly than in ssAnPRT-D83G + F149S and probably also ssAnPRT-wt. In contrast, in the activated variant ssAnPRT-D83G + F149S phosphoribosyl transfer ($k_{trans}$ = 28.3 $s^{-1}$) and PRA release ($k_{off}$ = 25.0 $s^{-1}$) contribute equally to the overall rate of forward catalysis ($k_{cat}$ = 13.3 $s^{-1}$).

For the synthesis reaction to proceed, the two substrates anthranilate and Mg·PRPP must be brought together, probably by means of a hinge motion where the N- and C-terminal domains close upon each other. Indeed, SAXS measurements with ssAnPRT-wt indicate that the enzyme undergoes a noticeable compaction upon full occupancy of its active site (*26*). This finding suggests that the inherent flexibility of the hinge region is central to the catalytic function of ssAnPRT, for example, by limiting the rate of product release from ssAnPRT-wt at 37 °C. In ssAnPRT-D83G + F149S, the extended binding mode of PRPP causes this substrate to span into the α-helical, N-terminal domain of the enzyme, approaching closely the binding sites for anthranilate. This change is caused by the D83G mutation, and as a consequence, a less extensive domain motion might be required for effective catalysis. Since F149S is located within the hinge between the two domains of the enzyme, it is likely that the substitution at this position has an influence on the dynamics of domain opening and closure movements. It has been shown that in cases where product release is rate-limiting, an increase in flexibility along a release channel can go along with an increased catalytic rate, especially when product dissociation occurs in the millisecond range (for ssAnPRT-D83G + F149S: $k_{off}$ = 25 $s^{-1}$, $t_{1/2}$ = 28 ms), a time scale that is similar to that expected for large amplitude segmental motions (*58*). For ssAnPRT-wt, the $k_{cat}$ value increases from 0.33 $s^{-1}$ at 37 °C to 4.2 $s^{-1}$ at 60 °C (*26*), suggesting that the velocity of product release, which limits the activity of the wild-type protein at 37 °C, is accelerated at 60 °C by a similar increase in flexibility as effected by the F149S replacement at 37 °C. Indeed, the melting temperature of ssAnPRT-D83G + F149S is decreased by ~10 °C compared to ssAnPRT-wt, and kinetic stability is decreased to ~10% of wild-type stability, which indicates an overall destabilization of the enzyme and might go hand in hand with increased flexibility. A similar effect has been observed with an activated variant of indole-3-glycerol phosphate synthase from *S. solfataricus*, which also shows an increased $k_{cat}$ value due to an increased product release rate (*8*). This variant is more rapidly inactivated and more prone to trypsin digestion than the wild-type enzyme, supporting an inverse correlation of thermal stability and conformational flexibility. Fluorescence resonance energy transfer measurements are under way to study the correlation between local dynamics and product release of ssAnPRT and its activated mutants in more detail.

## ACKNOWLEDGMENT

We thank Jeannette Ueckert for expert technical assistance, Dr. Marco Bocola and Harald Guldan for help with generation of figures, and Dr. Jochen Reinstein and Prof. Frank M. Raushel for discussion and advice.

## SUPPORTING INFORMATION AVAILABLE

Amino acid exchanges of ssAnPRT mutants isolated by *in vivo* complementation at 37 °C (Table S1), parameter estimates and confidence intervals for the best fit to equilibrium equations of the ligand binding model outlined in Experimental Procedures (Table S2), X-ray diffraction and model refinement statistics of ssAnPRT-D83G + F149S (Table S3), coordination distances between the pyrophosphate group of PRPP and metals in ssAnPRT-D83G + F149S (Table S4), and stereo representations of ligands bound to ssAnPRT-D83G + F149S and their corresponding electron density maps (Figure S1). This material is available free of charge via the Internet at http://pubs.acs.org.

## REFERENCES


1. Arnold, F. H., Wintrode, P. L., Miyazaki, K., and Gershenson, A. (2001) How enzymes adapt: lessons from directed evolution. *Trends Biochem. Sci. 26*, 100–106.
2. Sterner, R., and Liebl, W. (2001) Thermophilic adaptation of proteins. *Crit. Rev. Biochem. Mol. Biol. 36*, 39–106.
3. Jaenicke, R. (1991) Protein stability and molecular adaptation to extreme conditions. *Eur. J. Biochem. 202*, 715–728.
4. Miyazaki, K., Wintrode, P. L., Grayling, R. A., Rubingh, D. N., and Arnold, F. H. (2000) Directed evolution study of temperature adaptation in a psychrophilic enzyme. *J. Mol. Biol. 297*, 1015–1026.
5. Henn-Sax, M., Thoma, R., Schmidt, S., Hennig, M., Kirschner, K., and Sterner, R. (2002) Two $(\beta\alpha)_8$-barrel enzymes of histidine and tryptophan biosynthesis have similar reaction mechanisms and common strategies for protecting their labile substrates. *Biochemistry 41*, 12032–12042.
6. Sterner, R., Kleemann, G. R., Szadkowski, H., Lustig, A., Hennig, M., and Kirschner, K. (1996) Phosphoribosyl anthranilate isomerase from *Thermotoga maritima* is an extremely stable and active homodimer. *Protein Sci. 5*, 2000–2008.
7. Lönn, A., Gardonyi, M., van Zyl, W., Hahn-Hagerdal, B., and Otero, R. C. (2002) Cold adaptation of xylose isomerase from *Thermus thermophilus* through random PCR mutagenesis. Gene cloning and protein characterization. *Eur. J. Biochem. 269*, 157–163.
8. Merz, A., Yee, M. C., Szadkowski, H., Pappenberger, G., Crameri, A., Stemmer, W. P., Yanofsky, C., and Kirschner, K. (2000) Improving the catalytic activity of a thermophilic enzyme at low temperatures. *Biochemistry 39*, 880–889.
9. Nagatani, R. A., Gonzalez, A., Shoichet, B. K., Brinen, L. S., and Babbitt, P. C. (2007) Stability for function trade-offs in the enolase superfamily "catalytic module". *Biochemistry 46*, 6688–6695.
10. Shoichet, B. K., Baase, W. A., Kuroki, R., and Matthews, B. W. (1995) A relationship between protein stability and protein function. *Proc. Natl. Acad. Sci. U.S.A. 92*, 452–456.
11. Tokuriki, N., Stricher, F., Serrano, L., and Tawfik, D. S. (2008) How protein stability and new functions trade off. *PLoS Comput. Biol. 4*, e1000002.
12. Wray, J. W., Baase, W. A., Lindstrom, J. D., Weaver, L. H., Poteete, A. R., and Matthews, B. W. (1999) Structural analysis of a noncontiguous second-site revertant in T4 lysozyme shows that increasing the rigidity of a protein can enhance its stability. *J. Mol. Biol. 292*, 1111–1120.
13. Giver, L., Gershenson, A., Freskgard, P. O., and Arnold, F. H. (1998) Directed evolution of a thermostable esterase. *Proc. Natl. Acad. Sci. U.S.A. 95*, 12809–12813.
14. Hirano, N., Haruki, M., Morikawa, M., and Kanaya, S. (2000) Enhancement of the enzymatic activity of ribonuclease HI from *Thermus thermophilus* HB8 with a suppressor mutation method. *Biochemistry 39*, 13285–13294.
15. Stevenson, B. J., Liu, J. W., and Ollis, D. L. (2008) Directed evolution of yeast pyruvate decarboxylase 1 for attenuated regulation and increased stability. *Biochemistry 47*, 3013–3025.
16. Van den Burg, B., Vriend, G., Veltman, O. R., Venema, G., and Eijsink, V. G. (1998) Engineering an enzyme to resist boiling. *Proc. Natl. Acad. Sci. U.S.A. 95*, 2056–2060.
17. Williams, J. C., Zeelen, J. P., Neubauer, G., Vriend, G., Backmann, J., Michels, P. A., Lambeir, A. M., and Wierenga, R. K. (1999) Structural and mutagenesis studies of *Leishmania* triosephosphate isomerase: a point mutation can convert a mesophilic enzyme into a superstable enzyme without losing catalytic power. *Protein Eng. 12*, 243–250.
18. Yasugi, M., Amino, M., Suzuki, T., Oshima, T., and Yamagishi, A. (2001) Cold adaptation of the thermophilic enzyme 3-isopropylmalate dehydrogenase. *J. Biochem. (Tokyo) 129*, 477–484.
19. Sinha, S. C., and Smith, J. L. (2001) The PRT protein family. *Curr. Opin. Struct. Biol. 11*, 733–739.
20. Ozturk, D. H., Dorfman, R. H., Scapin, G., Sacchettini, J. C., and Grubmeyer, C. (1995) Locations and functional roles of conserved lysine residues in *Salmonella typhimurium* orotate phosphoribosyltransferase. *Biochemistry 34*, 10755–10763.
21. Scapin, G., Ozturk, D. H., Grubmeyer, C., and Sacchettini, J. C. (1995) The crystal structure of the orotate phosphoribosyltransferase complexed with orotate and α-D-5-phosphoribosyl-1-pyrophosphate. *Biochemistry 34*, 10744–10754.
22. Schumacher, M. A., Bashor, C. J., Song, M. H., Otsu, K., Zhu, S., Parry, R. J., Ullman, B., and Brennan, R. G. (2002) The structural mechanism of GTP stabilized oligomerization and catalytic activation of the *Toxoplasma gondii* uracil phosphoribosyltransferase. *Proc. Natl. Acad. Sci. U.S.A. 99*, 78–83.
23. Craig, S. P.III, and Eakin, A. E. (2000) Purine phosphoribosyltransferases. *J. Biol. Chem. 275*, 20231–20234.
24. Cao, H., Pietrak, B. L., and Grubmeyer, C. (2002) Quinolinate phosphoribosyltransferase: kinetic mechanism for a type II PRTase. *Biochemistry 41*, 3520–3528.
25. Eads, J. C., Ozturk, D., Wexler, T. B., Grubmeyer, C., and Sacchettini, J. C. (1997) A new function for a common fold: the crystal structure of quinolinic acid phosphoribosyltransferase. *Structure 5*, 47–58.
26. Marino, M., Deuss, M., Svergun, D. I., Konarev, P. V., Sterner, R., and Mayans, O. (2006) Structural and mutational analysis of substrate complexation by anthranilate phosphoribosyltransferase from *Sulfolobus solfataricus*. *J. Biol. Chem. 281*, 21410–21421.
27. Mayans, O., Ivens, A., Nissen, L. J., Kirschner, K., and Wilmanns, M. (2002) Structural analysis of two enzymes catalysing reverse metabolic reactions implies common ancestry. *EMBO J. 21*, 3245–3254.
28. Kim, C., Xuong, N. H., Edwards, S., Madhusudan, Yee, M. C., Spraggon, G., and Mills, S. E. (2002) The crystal structure of anthranilate phosphoribosyltransferase from the enterobacterium *Pectobacterium carotovorum*. *FEBS Lett. 523*, 239–246.
29. Lee, C. E., Goodfellow, C., Javid-Majd, F., Baker, E. N., and Shaun Lott, J. (2006) The crystal structure of TrpD, a metabolic enzyme essential for lung colonization by *Mycobacterium tuberculosis*, in complex with its substrate phosphoribosylpyrophosphate. *J. Mol. Biol. 355*, 784–797.
30. Schwab, T., Skegro, D., Mayans, O., and Sterner, R. (2008) A rationally designed monomeric variant of anthranilate phosphoribosyltransferase from *Sulfolobus solfataricus* is as active as the dimeric wild-type enzyme but less thermostable. *J. Mol. Biol. 376*, 506–516.
31. Ivens, A., Mayans, O., Szadkowski, H., Wilmanns, M., and Kirschner, K. (2001) Purification, characterization and crystallization of thermostable anthranilate phosphoribosyltransferase from *Sulfolobus solfataricus*. *Eur. J. Biochem. 268*, 2246–2252.
32. Stemmer, W. P. (1994) DNA shuffling by random fragmentation and reassembly: in vitro recombination for molecular evolution. *Proc. Natl. Acad. Sci. U.S.A. 91*, 10747–10751.
33. Jürgens, C., Strom, A., Wegener, D., Hettwer, S., Wilmanns, M., and Sterner, R. (2000) Directed evolution of a $(\beta\alpha)_8$-barrel enzyme to catalyze related reactions in two different metabolic pathways. *Proc. Natl. Acad. Sci. U.S.A. 97*, 9925–9930.
34. Yanofsky, C., and Horn, V. (1981) Rifampin resistance mutations that alter the efficiency of transcription termination at the tryptophan operon attenuator. *J. Bacteriol. 145*, 1334–1341.
35. Vogel, H. J., and Bonner, D. M. (1956) Acetylornithinase of *Escherichia coli*: Partial purification and some properties. *J. Biol. Chem. 218*, 97–106.
36. Ho, S. N., Hunt, H. D., Horton, R. M., Pullen, J. K., and Pease, L. R. (1989) Site-directed mutagenesis by overlap extension using the polymerase chain reaction. *Gene 77*, 51–59.
37. Horton, R. M., Hunt, H. D., Ho, S. N., Pullen, J. K., and Pease, L. R. (1989) Engineering hybrid genes without the use of restriction enzymes: gene splicing by overlap extension. *Gene 77*, 61–68.
38. Pace, C. N., Vajdos, F., Fee, L., Grimsley, G., and Gray, T. (1995) How to measure and predict the molar absorption coefficient of a protein. *Protein Sci. 4*, 2411–2423.
39. Kuzmic, P. (1996) Program DYNAFIT for the analysis of enzyme kinetic data: application to HIV proteinase. *Anal. Biochem. 237*, 260–273.
40. Thompson, R. E., Li, E. L., Spivey, H. O., Chandler, J. P., Katz, A. J., and Appleman, J. R. (1978) Apparent stability constants of $H^+$ and $Mg^{2+}$ complexes of 5-phosphoribosyl α-1-pyrophosphate. *Bioinorg. Chem. 9*, 35–45.

41. Stoll, V. S., and Blanchard, J. S. (1990) Buffers: principles and practice. *Methods Enzymol. 182*, 24–38.
42. Kabsch, W. (1993) Automatic processing of rotation diffraction data from crystals of initially unknown symmetry and cell constants. *J. Appl. Crystallogr. 26*, 795–800.
43. McCoy, A. J. (2007) Solving structures of protein complexes by molecular replacement with Phaser. *Acta Crystallogr., Sect. D: Biol. Crystallogr. 63*, 32–41.
44. Murshudov, G. N., Vagin, A. A., and Dodson, E. J. (1997) Refinement of macromolecular structures by the maximum-likelihood method. *Acta Crystallogr., Sect. D: Biol. Crystallogr. 53*, 240–255.
45. Emsley, P., and Cowtan, K. (2004) Coot: model-building tools for molecular graphics. *Acta Crystallogr., Sect. D: Biol. Crystallogr. 60*, 2126–2132.
46. Collaborative Computational Project, N. (1994) The CCP4 suite: programs for protein crystallography. *Acta Crystallogr., Sect. D: Biol. Crystallogr. 50*, 760–763.
47. Stemmer, W. P. (1994) Rapid evolution of a protein *in vitro* by DNA shuffling. *Nature 370*, 389–391.
48. Grogan, D. W. (1989) Phenotypic characterization of the archaebacterial genus *Sulfolobus*: comparison of five wild-type strains. *J. Bacteriol. 171*, 6710–6719.
49. Salerno, C., and Giacomello, A. (1981) Human hypoxanthine guanine phosphoribosyltransferase. The role of magnesium ion in a phosphoribosylpyrophosphate-utilizing enzyme. *J. Biol. Chem. 256*, 3671–3673.
50. Hommel, U., Lustig, A., and Kirschner, K. (1989) Purification and characterization of yeast anthranilate phosphoribosyltransferase. *Eur. J. Biochem. 180*, 33–40.
51. Bicknell, R., and Waley, S. G. (1985) Single-turnover and steady-state kinetics of hydrolysis of cephalosporins by beta-lactamase I from *Bacillus cereus*. *Biochem. J. 231*, 83–88.
52. Fierke, C. A., and Hammes, G. G. (1995) Transient kinetic approaches to enzyme mechanisms. *Methods Enzymol. 249*, 3–37.
53. Hurwitz, C., and Rosano, C. L. (1967) The intracellular concentration of bound and unbound magnesium ions in *Escherichia coli*. *J. Biol. Chem. 242*, 3719–3722.
54. Gross, J. W., Rajavel, M., and Grubmeyer, C. (1998) Kinetic mechanism of nicotinic acid phosphoribosyltransferase: implications for energy coupling. *Biochemistry 37*, 4189–4199.
55. Wang, G. P., Lundegaard, C., Jensen, K. F., and Grubmeyer, C. (1999) Kinetic mechanism of OMP synthase: A slow physical step following group transfer limits catalytic rate. *Biochemistry 38*, 275–283.
56. Xu, Y., Eads, J., Sacchettini, J. C., and Grubmeyer, C. (1997) Kinetic mechanism of human hypoxanthine-guanine phosphoribosyltransferase: Rapid phosphoribosyl transfer chemistry. *Biochemistry 36*, 3700–3712.
57. Chappie, J. S., Canaves, J. M., Han, G. W., Rife, C. L., Xu, Q., and Stevens, R. C. (2005) The structure of a eukaryotic nicotinic acid phosphoribosyltransferase reveals structural heterogeneity among type II PRTases. *Structure 13*, 1385–1396.
58. Codreanu, S. G., Ladner, J. E., Xiao, G., Stourman, N. V., Hachey, D. L., Gilliland, G. L., and Armstrong, R. N. (2002) Local protein dynamics and catalysis: detection of segmental motion associated with rate-limiting product release by a glutathione transferase. *Biochemistry 41*, 15161–15172.